PHYSICAL REVIEW E **79**, 030906(R) (2009)

Line-defect patterns of unstable spiral waves in cardiac tissue

Juan G. Restrepo[1,*] and Alain Karma[2]
[1]*Department of Applied Mathematics, University of Colorado, Boulder, Colorado 80309, USA*
[2]*Department of Physics and Center for Interdisciplinary Research on Complex Systems, Northeastern University, Boston, Massachusetts 02115, USA*

(Received 20 June 2008; revised manuscript received 6 October 2008; published 30 March 2009)

Spiral wave propagation in period-2 excitable media is accompanied by line defects, the locus of points with period-1 oscillations. Here we investigate spiral line defects in cardiac tissue where period-2 behavior has a known arrhythmogenic role. We find that the number of line defects, which is constrained to be an odd integer, is 3 for a freely rotating spiral, with and without meander, but 1 for a spiral anchored around a fixed heterogeneity. We interpret this finding analytically using a simple theory where spiral wave unstable modes with different numbers of line defects correspond to quantized solutions of a Helmholtz equation. Furthermore, the slow inward rotation of spiral line defects is described in different regimes.

DOI: 10.1103/PhysRevE.79.030906 PACS number(s): 87.19.Hh, 47.54.−r, 05.45.Xt

Spiral waves are observed in extremely diverse physical and biological excitable media and are known to play a key role in the genesis of abnormally rapid life-threatening heart rhythm disorders [1]. Despite considerable progress to date, complex spatiotemporal behaviors resulting from unstable spiral wave propagation remain poorly understood theoretically, with the exception of meander [2,3], a classic spiral core instability with flowerlike tip trajectories. A particularly rich dynamics results from instabilities in period-2 media where the local dynamics of the medium, i.e., the dynamics of uncoupled excitable elements, exhibits a period-doubling bifurcation as a function of parameters of the medium or the external stimulation frequency. Although period-2 behavior has been observed in different excitable and oscillatory media, it has received particular attention in a cardiac context. The hallmark of period-2 behavior in this context is alternans, a beat-to-beat alternation in the duration of cardiac excitation, which has been linked to the onset of lethal heart rhythm disorders [4].

Unstable spiral wave propagation in period-2 media is invariably accompanied by "line defects," which are the locus of points where the dynamics is locally period 1. Line defects were first observed in computer simulations of coupled oscillators [5,6] and subsequently in Belousov-Zhabotinsky (BZ) reaction experiments [7–9] and *in vitro* cardiac cell tissue cultures [10,11]. Computer simulations also predicted the existence of line-defect turbulence and phase bubbles [12], which were later observed in BZ reaction experiments [13,14] (see [15] for a review). Here we study the dynamics of line defects in cardiac action propagation models. Local period-2 dynamics has been hypothesized in this context as a potential mechanism for heart fibrillation [1,16–18] by inducing spiral wave breakup. Despite recent studies of period-2 spiral wave bifurcations [19], spiral line-defect patterns have not been systematically investigated in cardiac tissue. In this Rapid Communication, we investigate the selection and dynamics of line-defect patterns resulting from unstable spiral wave propagation in cardiac tissue. Moreover, we interpret our findings using an amplitude equation framework recently used to study the evolution of line defects during periodic stimulation from a single site [20]. In this framework, the spatiotemporal modulation of the phase and amplitude of period-2 oscillations is described by a simple partial differential equation that can be readily analyzed. Our study is based on the standard wave equation for cardiac tissue,

$$\partial_t V = \gamma \nabla^2 V - I_m(V,\vec{y})/C_m, \tag{1}$$

where V is the transmembrane voltage, γ is the voltage diffusion coefficient, C_m is the membrane capacitance, and $\vec{y}$ is a vector of gate variables that controls the flow of ions through the membrane, and hence the total membrane ionic current I_m. We studied different models of $I_m(V,\vec{y})$ and gating kinetics to explore universal features of line-defect patterns that depend on qualitative properties of core and plane wave instabilities. The latter are manifested either as *stationary* [20,21] or *traveling* [20] spatial modulations of period-2 oscillation amplitude with an intrinsic spatial scale determined by parameters of the excitable medium [20]. These spatial modulations have nodes with period-1 dynamics in one dimension, or nodal lines in two, which correspond here to line defects in the spiral far field. We therefore chose models to explore line-defect patterns for stationary and traveling nodes with and without meander. The model of Ref. [17] has pinwheel spirals (no meander) and stationary nodes under periodic pacing. The other two models of Ref. [22] and Ref. [20] both exhibit meander and have fixed and traveling nodes, respectively.

Freely propagating spiral waves in all three models were studied by numerically solving Eq. (1) in a circular domain of radius $r_e=3$ cm with no-flux boundary conditions, $\partial_r V|_{r=r_e}=0$. Anchored spirals were studied by introducing an inexcitable disk of radius r_i and imposing no-flux conditions on both the inner and outer radii, $\partial_r V|_{r=r_i}=\partial_r V|_{r=r_e}=0$. We implemented the phase-field method of Ref. [23] which automatically handles no-flux boundary conditions in an arbitrary geometry using a finite-difference representation of the Laplacian on a square grid, and iterated Eq. (1) using a simple explicit Euler scheme. Model parameters are identical to the published ones except those listed in the caption of

*juanga@colorado.edu

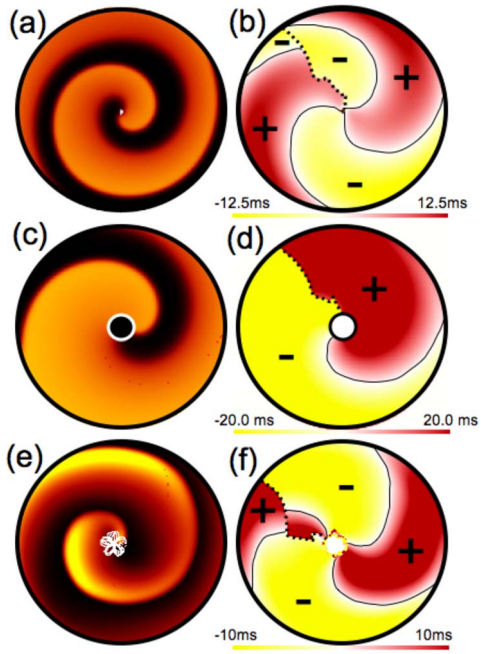

FIG. 1. (Color online) Membrane voltage (left) and corresponding alternans amplitude a (right) for different ionic models and geometries: model of Ref. [17] without [(a) and (b); Re=1.15] and with a circular inexcitable disk of radius r_i=0.5 cm [(c) and (d); Re=1.25], and model of Ref. [22] without disk [(e) and (f); t_{f2} =30 ms, t_{si}=10 ms, t_{h2}=2.0 ms]. In (a), (c), and (e), gray (orange online) indicates depolarization, and white indicates the trajectory of the spiral tip. In (b), (d), and (f), dark gray (red online) and light gray (yellow online) correspond to $a>0$ and $a<0$ regions, separated by line defects (solid lines); the gray (color online) scale does not vary outside the indicated range of a. Line defects in (b), (d), and (f) rotate counterclockwise with a period that is approximately 17, 8, and 9 times the clockwise spiral rotation period in (a), (c), and (e), respectively. The discontinuity of a across the dashed line is a consequence of the definition of the common beat number (see text).

Fig. 1. The latter were chosen for intermediate action potential duration restitution slopes, which suffice to produce unstable spiral waves with line defects in each geometry, but are not steep enough to cause wave breakup in this domain size.

We used a half plane wave as the initial condition to initiate a spiral wave (obtained by first triggering a full plane wave and resetting part of the circular domain to the resting state). To track line defects, we define at each point $\mathbf{x}$ and time t a local beat number $n(\mathbf{x},t)$, set everywhere initially to zero after the half plane wave is created, and increased by one at the end of each action potential, i.e., every time that the voltage $V(\mathbf{x},t)$ crosses a fixed threshold V_c with $dV/dt<0$. We then define the period-2 alternans amplitude as

$$a(\mathbf{x},t) = (-1)^{n_c(t)}[D(\mathbf{x},n_c(t)) - D(\mathbf{x},n_c(t)-1)]/2, \quad (2)$$

where $D(\mathbf{x},n)=\int_{V(\mathbf{x},t')>V_c,n(\mathbf{x},t')=n-1}dt'$ is the local action potential duration (APD) and $n_c(t)\equiv\min_{\mathbf{x}}n(\mathbf{x},t)$ is the common beat, i.e., the largest beat number that has been registered at all points at time t. The line defects are then the locus of points where $a(\mathbf{x},t)=0$ at any instant of time. The use of a common beat number introduces here a discontinuity in a (indicated by dashed lines in Fig. 1) since the APD of a given beat might change as the wave front rotates around the spiral tip. This discontinuity, however, does not affect the dynamics. Other methods to track line defects [7,24] yield similar results except for inessential imaging differences.

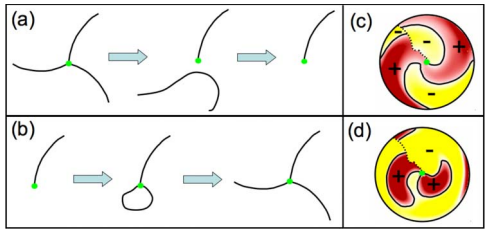

FIG. 2. (Color online) Schematic illustration of transitions from (a) three to one and (b) one to three line defects and corresponding examples from simulations of the model of Ref. [17] with the same conventions and parameters as in Fig. 1(b). The small circle (green online) in (a) and (b) represents the spiral core region or a small anchoring obstacle.

Results of simulations that pertain to the selection of the number of line defects are shown in Fig. 1. The top four panels reveal that the pinwheel spirals simulated with the two-variable model of Ref. [17] exhibit three line defects when propagating freely in spatially homogeneous tissue, but only one line defect when anchored around an inexcitable disk of 0.5 cm radius. Furthermore, the bottom two panels show that, for the more physiologically realistic three-variable model of Ref. [22], freely propagating spirals still exhibit three line defects even though the spiral tip meanders. We have repeated these simulations in domains of different sizes and shapes and confirmed that the results do not depend on the particular geometry we are showing. In addition, the results are robust to the presence of other spirals.

Since anchored spirals become free in the limit of vanishing obstacle size, one would expect transitions from one to three (three to one) line defects to occur with decreasing (increasing) obstacle size. Indeed, for the model of Ref. [17], we found three line defects for obstacles with diameter smaller than ~0.1 cm, including the freely propagating pinwheel spiral (r_i=0) in Fig. 1(b), and one line defect for diameters larger than ~0.3 cm as in the example of Fig. 1(d). For intermediate diameters, we found complex behaviors marked by transitions from three to one or one to three line defects, as illustrated in Fig. 2.

Let us now turn to interpret our results in the amplitude equation framework. We restrict our analysis to nonmeandering spiral waves. We will use a simplified version of the amplitude equation describing the spatiotemporal dynamics of alternans in two-dimensional tissue derived in [20] [Eq. (78)]. Assuming a constant conduction velocity, diffusive coupling independent of the direction of propagation of the wave front, and keeping only linear terms in a, the full amplitude equation presented in [20] reduces to

$$T\partial_t a = \sigma a + \xi^2\nabla^2 a. \quad (3)$$

The alternans amplitude a is subject to the radial $\partial_r a|_{r_i} = \partial a|_{r_e}=0$ and angular $a(\theta+2\pi,t)=-a(\theta,t)$ boundary condi-

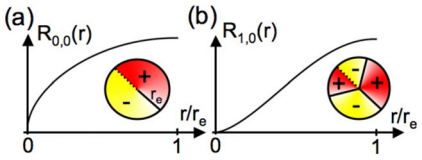

FIG. 3. (Color online) Theoretical radial and angular (insets) dependence of the alternans amplitude for (a) one and (b) three line defect modes.

tions. The latter constrains the number of line defects to be an odd integer and results from the change in beat number across any closed circuit enclosing the spiral tip for steady-state alternans. It follows directly from the definition of a [Eq. (2)] and the requirement that the voltage be continuous everywhere in space. In addition, $\sigma=\ln f'$, where f', the slope of the action potential duration restitution curve defined by $D^{n+1}=f(T-D^n)$, controls the onset of alternans and $\xi\sim(\gamma D)^{1/2}$, where D is the value of the action potential duration at the period-doubling bifurcation ($\sigma=0$), measures the scale over which the voltage dynamics is diffusively coupled on the time scale of one beat.

This linear stability problem is easily solved by the substitution $a(\mathbf{r},t)\sim e^{\Omega t}\Psi(r,\theta)$ which transforms Eq. (3) into a Helmholtz equation for $\Psi(r,\theta)$. The latter can then be solved by separation of variables with the substitution $\Psi(r,\theta)\sim R(r)\Theta(\theta)$. The angular part is found to be $\Theta_n(\theta)=\sin[(n+1/2)\theta]$, where mode n corresponds to $2n+1$ line defects. The radial part obeys a Bessel equation. For $r_i>0$, it has solutions $R_{n,m}(r)\propto J'_{-n-1/2}(k_{n,m}r_e)J_{n+1/2}(k_{n,m}r)-J'_{n+1/2}(k_{n,m}r_e)J_{-n-1/2}(k_{n,m}r)$ that satisfy the outer radial boundary condition $\partial a|_{r_e}=0$, where $n,m=0,1,\ldots$, and the inner condition $\partial_r a|_{r_i}=0$ determines $k_{n,m}$, and hence the growth rate $\Omega_{n,m}T=\sigma-\xi r_e^{-2}k_{n,m}^2$. We find that the smallest $k_{n,m}$ occurs for $n=0$ independently of the ratio r_e/r_i. Therefore, the mode corresponding to a single line defect is the most unstable when the spiral is anchored. This agrees with our numerical observations in Fig. 1(d). For freely rotating spirals, $r_i=0$, $J_{-n-1/2}(r)$ diverges at the origin, so the solutions are $R_{n,m}(r)\propto J_{n+1/2}(k_{n,m}r)$, where $k_{nm}r_e$ is the mth zero of $J'_n(r)$. The most unstable modes are, in this order, $n=0$ and $n=1$, corresponding to one and three line defects, respectively (see Fig. 3). However, $J_{1/2}(k_{0,0}r)$ has a divergent derivative at the origin that is incompatible with the physical requirement that the voltage, and hence the APD, must vary smoothly on a scale ξ in cardiac tissue. This requirement follows from the fact that "thick" spirals generically form in cardiac tissue for normal excitability, meaning that the angular distance between the spiral wave front and wave back increases with r on a scale larger than ξ, as is apparent in Fig. 1(a). For weak excitability, in contrast, "thin" spirals are formed where the distance between front and back becomes constant at a distance $r\sim\xi$ from the core. In this case, the alternans amplitude can be finite at a distance $r\sim\xi$ and hence lead to a boundary condition on the outer scale $r\gg\xi$ of the spiral pattern where a is finite in the core. Such a boundary condition favors the selection of one line defect as in the case of anchored spirals, and we have indeed observed free spirals with one line defect for weakly excitable parameter ranges of the two-variable model of Ref. [17]. It is also reasonable to conjecture that the selection of one line defect in some oscillatory media (e.g., [6]) is due to the formation of thin spirals in these media, where period-2 oscillations extend into the core region $r\sim\xi$ as for weakly excitable cardiac spirals. From this standpoint, the selection of three line defects for thick spirals in cardiac tissue is a major result of our work in comparison to previous findings in other oscillatory media.

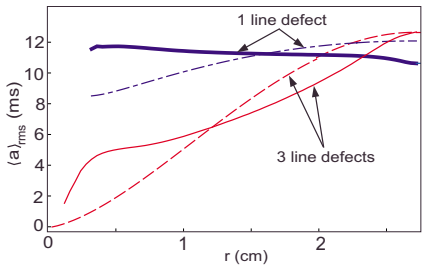

FIG. 4. (Color online) $\langle a\rangle_{\mathrm{rms}}$ versus radial distance r for the pinwheel spiral (thin solid line, red online) and anchored spiral (thick solid line, blue online), and respective theoretical radial modes $R_{1,0}(r)$ (thin dashed, red online) and $R_{0,0}(r)$ (dotted-dashed line, blue online).

Interestingly, a three-line-defect pattern is also selected with meander present [Fig. 1(f)], thereby suggesting that the boundary condition on a on the outer scale of the line-defect pattern is not strongly affected by meander. However, since our theory does not apply to meandering spirals, this case remains open to future theoretical study.

The analysis also predicts qualitative features of the radial distribution of alternans amplitude for three- and one-line-defect patterns of Figs. 1(b) and 1(d), respectively. Figure 4 compares the numerical radial distributions of root-mean-square amplitude $\langle a\rangle_{\mathrm{rms}}$ averaged over a full line-defect rotation period for three line defects (thin solid line) and one line defect (thick line), with the corresponding radial modes from the theoretical analysis (dashed lines) scaled to have the same radial average as the observed curves. The theory predicts well that the alternans amplitude is more strongly suppressed near the core for a larger number of line defects.

So far our analysis has assumed that the wave speed is constant, which predicts that line defects extend straight out of the core and are stationary, as implied by the angular distribution $\sin[(n+1/2)\theta]$ of linearly unstable modes (see Fig. 3). In contrast, the simulations in Fig. 1 show that line defects have a spiral shape and slowly rotate inward in the opposite direction to the spiral wave front. Line-defect motion can generally be induced by both line-defect curvature and the dependence of the wave speed c on the interval I between two waves, known as the conduction velocity (CV) restitution curve in the cardiac literature. While a full stability analysis that includes these effects would be required to treat line-defect motion in general, two important limiting cases can be readily analyzed.

The first pertains to anchored spiral waves for medium parameters where plane waves paced at the spiral rotation period exhibit stationary line defects, as for the model of Ref. [17] studied here. In this case, we expect line-defect motion to be generated predominantly by the spiral wave front dynamics around the anchoring obstacle. Neglecting

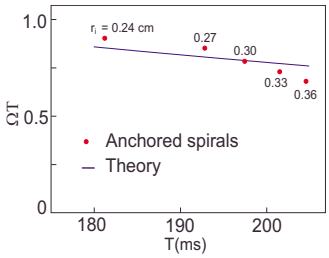

FIG. 5. (Color online) Comparison of numerical (circles, red online) and theoretical (solid line) line-defect rotation frequencies for spiral waves anchored to disks of varying radii for the model of Ref. [17].

wave front curvature effects, this dynamics should be approximately described by that of a propagating pulse in a one-dimensional ring of perimeter $L=2\pi r_i$ [20,25]. To test this hypothesis, we computed the quasiperiodic frequency Ω of the local medium dynamics induced by line-defect rotation for anchored spirals for the model of Ref. [17]. The frequency was obtained by fitting the time series $a(\mathbf{r},jT)/a(\mathbf{r},0)$ at a single point $\mathbf{r}$ to $\eta^j \cos(\Omega T j+\delta)$, with η, Ω, and δ the fitting parameters. For the theory, we used the dispersion relation giving the quasiperiodic frequency Ω modulating alternans, $a \propto e^{i\Omega jT}$, in a one-dimensional ring derived in Ref. [20],

$$e^{i\Omega T}(1-i/2\Lambda k)=(1-iwk-\xi^2k^2)f'(I)+i/2\Lambda k, \qquad (4)$$

where $k=\pi/L+\Omega T/L$ is the wave number corresponding to a single line defect and $\Lambda=c'(I)/(2c^2)$. The APD and CV restitution curves $f(I)$ and $c(I)$ were calculated in a one-dimensional cable as in Ref. [20]. In addition, the intercellular coupling parameters ω and ξ were estimated as $\omega \sim 2\gamma/c$ and $\xi \sim (\gamma D)^{1/2}$ [20]. The comparison in Fig. 5 shows that the ring-based theory predicts reasonably well the frequency of line-defect rotation for anchored spiral waves of different period T, which was varied here by increasing the obstacle radius r_i in the simulations.

The opposite limit that can also be readily understood is the one where plane waves paced at the spiral rotation period exhibit line defects that move toward the pacing site, which generally occurs for steeper CV restitution. In this case, line-defect motion is expected to be dominated by the far-field spiral dynamics [20]. We have checked that, for the two-variable model of Ref. [20], spiral line defects indeed rotate inward with a frequency equal to the product of the velocity of the planar line defects and the inverse of their spacing. This property was purposely checked in a domain much larger than the spiral wavelength ($r_e=18$ cm) and with an obstacle size ($r_i=0.72$ cm) sufficient to prevent spiral wave breakup inherent in this model. However, we expect this behavior to be generic for systems with traveling planar line defects and to also apply to freely rotating spirals with three line defects for parameters where breakup does not occur.

In summary, we have surveyed spiral line-defect patterns in simplified models of cardiac excitation with period-2 dynamics. Although far from exhaustive, this survey yields the striking finding that freely propagating and anchored spiral waves select different numbers of line defects. This opens up the possibility to distinguish free and anchored spiral waves in cardiac tissue by monitoring the number of line defects. We have shown that spiral wave unstable modes with different numbers of line defects correspond to topologically quantized solutions of a Helmholtz equation. In this framework, the boundary condition on the period-2 oscillation amplitude in the spiral core, which is fundamentally different for free and anchored spirals, selects the number of line defects. Furthermore, we have found that line-defect inward rotation can be driven either by the core or by far-field wave front dynamics, with concomitantly different frequencies.

We thank Blas Echebarria for valuable discussions. This work was supported by NIH Grant No. P01 HL078931.

[1] J. N. Weiss *et al.*, Circulation **112**, 1232 (2005).
[2] D. Barkley, Phys. Rev. Lett. **68**, 2090 (1992).
[3] V. Hakim and A. Karma, Phys. Rev. Lett. **79**, 665 (1997); Phys. Rev. E **60**, 5073 (1999).
[4] A. Karma and R. F. Gilmour, Phys. Today **60** (3), 51 (2007); J. N. Weiss *et al.*, Circ. Res. **98**, 1244 (2006).
[5] A. Goryachev and R. Kapral, Phys. Rev. E **54**, 5469 (1996).
[6] A. Goryachev, H. Chate, and R. Kapral, Phys. Rev. Lett. **80**, 873 (1998).
[7] J. S. Park and K. J. Lee, Phys. Rev. Lett. **88**, 224501 (2002); J. S. Park, S. J. Woo, and K. J. Lee, *ibid.* **93**, 098302 (2004); J. S. Park and K. J. Lee, Phys. Rev. E **73**, 066219 (2006).
[8] J. S. Park and K. J. Lee, Phys. Rev. Lett. **83**, 5393 (1999).
[9] B. Marts, D. J. W. Simpson, A. Hagberg, and A. Lin, Phys. Rev. E **76**, 026213 (2007).
[10] S. M. Hwang *et al.*, Proc. Natl. Acad. Sci. U.S.A. **102**, 10363 (2005).
[11] T. Y. Kim *et al.*, Proc. Natl. Acad. Sci. U.S.A. **104**, 11639 (2007).
[12] A. Goryachev *et al.*, Phys. Rev. Lett. **83**, 1878 (1999).
[13] J. S. Park and K. J. Lee, Phys. Rev. Lett. **83**, 5393 (1999).
[14] J. S. Park, S. J. Woo, O. Kwon, T. Y. Kim, and K. J. Lee, Phys. Rev. Lett. **100**, 068302 (2008).
[15] A. Goryachev *et al.*, Int. J. Bifurcation Chaos Appl. Sci. Eng. **10**, 1537 (2000).
[16] A. Karma, Phys. Rev. Lett. **71**, 1103 (1993).
[17] A. Karma, Chaos **4**, 461 (1994).
[18] F. H. Fenton *et al.*, Chaos **12**, 852 (2002).
[19] B. Sandstede and A. Scheel, SIAM J. Appl. Dyn. Syst. **6**, 494 (2007); D. Allexandre and N. F. Otani, Phys. Rev. E **70**, 061903 (2004).
[20] B. Echebarria and A. Karma, Phys. Rev. Lett. **88**, 208101 (2002); Phys. Rev. E **76**, 051911 (2007).
[21] M. A. Watanabe *et al.*, J. Cardiovasc. Electrophysiol. **12**, 196 (2001).
[22] B. Echebarria and A. Karma, Eur. Phys. J. Spec. Top. **46**, 217 (2007).
[23] F. Fenton *et al.*, Chaos **15**, 013502 (2005).
[24] M. Zhan and R. Kapral, Phys. Rev. E **72**, 046221 (2005).
[25] M. Courtemanche, L. Glass, and J. P. Keener, Phys. Rev. Lett. **70**, 2182 (1993).